Evolution of the Tropospheric Split Jet over the South Pacific Ocean during the 1986–89 ENSO Cycle*

BIAO CHEN, SHAWN R. SMITH,† AND DAVID H. BROMWICH@

Polar Meteorology Group, Byrd Polar Research Center, The Ohio State University, Columbus, Ohio

(Manuscript received 23 May 1995, in final form 14 February 1996)

ABSTRACT

A case study investigation into the meridional and horizontal circulation over the South Pacific Ocean is presented for the 1986–89 El Niño–Southern Oscillation (ENSO) cycle. Using the European Centre for Medium-Range Weather Forecasts (ECMWF) analyses, annual average fields are created for the years before and after the 1987 minimum (warm phase) and 1989 maximum (cold phase) in the Southern Oscillation index. The analyses reveal a shift in the split jet stream over the South Pacific sector (180°–120°W) from a strong subtropical jet (STJ) and weak polar front jet (PFJ) during the warm phase to a weak STJ and strong PFJ during the cold phase.

Analysis of the momentum budget reveals how the split jet in the upper troposphere over South Pacific Ocean evolved during the 1986–89 ENSO cycle. During the warm phase, the strong STJ is associated with advection of the mean flow momentum flux from the Australian sector, which is approximately balanced by a large negative ageostrophic term; the PFJ is primarily associated with eddy momentum convergence, which is partially counterbalanced by the ageostrophic term. During the cold phase, the weakened STJ is related to an increasingly negative ageostrophic term and a less positive mean flow momentum convergence. The strengthened PFJ is associated with an increase in the convergence of eddy momentum flux that is mainly composed of 2.5–6-day poleward momentum transport from midlatitudes and 7–30-day equatorward momentum transport from high latitudes. In general, the impacts of eddy stress on the STJ and the mean momentum divergence on the PFJ in this sector are small.

The variations in the split jet may reflect the poleward propagation of the ENSO signal via the South Pacific convergence zone. The implications for the high southern latitudes are discussed as interannual variations are found in the low-level easterlies near Antarctica and the Amundsen Sea low.

1. Introduction

The El Niño/Southern Oscillation (ENSO), described by Philander and Rasmusson (1985) as a coupled atmosphere–ocean phenomenon, has long been recognized as the major climate variation of the tropical South Pacific Ocean. However, though ENSO is centered in the tropical Pacific, many authors have found ENSO signals in far reaching regions of the globe. For example, Horel and Wallace (1981) found ENSO teleconnections in North America and van Loon and Madden (1981), Mo and White (1985), and Karoly (1989) found teleconnections over parts of the Southern Hemisphere. Savage et al. (1988) even discovered an ENSO signal at the South Pole. Smith and Stearns (1993) expanded on the work of Savage et al. (1988) and revealed significant correlations between a Tahiti-minus-Darwin sea level pressure (SLP) Southern Oscillation index (SOI) and the surface temperatures and pressures over the Antarctic continent. Others working in the south polar region have found ENSO signals in sea ice (Simmonds and Jacka 1995; Gloersen 1995; Carleton 1988), West Antarctic precipitation (work in progress), and populations of marine life (Testa et al. 1991). As a result of these and many other efforts, ENSO has become known as a global climate variation.

More recently, researchers have turned away from the search for global ENSO signals and focused more on the dynamic mechanisms that transmit the ENSO signal through the atmosphere. Held et al. (1989) suggested a process by which extratropical transients can be organized by tropical SST anomalies, a primary component of ENSO. They argued that a tropically forced wave train of only modest amplitude may be sufficient to displace the downstream portion of the oceanic storm track. In the Northern Hemisphere, Horel and Wallace (1981) indicated that the well-known Pacific–North American

* Contribution 995 of the Byrd Polar Research Center.

† Current affiliation: Center for Ocean Atmospheric Prediction Studies, Florida State University, Tallahassee, Florida.

@ Also affiliated with: Atmospheric Sciences Program, The Ohio State University, Columbus, Ohio.

Corresponding author address: Dr. David H. Bromwich, Byrd Polar Research Center, Ohio State University, 1090 Carmack Road, Columbus, OH 43210-1002.

(PNA) pattern transmits the ENSO signal to the United States. Furthermore, Hoerling and Ting (1994) found that the anomalous transient vorticity fluxes are remarkably robust over the North Pacific during each ENSO event from 1982 to 1993, with an eastward extension of the climatological storm track leading to strong cyclonic forcing near 40°N.

Due to the recent discoveries of ENSO signals in the south polar regions (Smith and Stearns 1993; Savage et al. 1988), this article focuses on a possible mechanism for transporting the ENSO signal poleward in the Southern Hemisphere. Karoly (1989) suggested that the Pacific–South American (PSA) pattern may fill the transport role. Vincent (1994) summarized the work of Trenberth (1976), Meehl (1987), and several other authors who suggested that the South Pacific convergence zone (SPCZ) may be related to variations in the ENSO cycle and may be a conduit for the poleward propagation of the ENSO signal. To further investigate the influence of ENSO in this area, this effort focuses on the split tropospheric jet stream (also known the double jet stream) climatologically located over Australia and the South Pacific Ocean (Taljaard et al. 1969). Though the split jet phenomenon in the Southern Hemisphere was found in the early 1970s (van Loon 1972), few studies have concentrated on the interannual variation of the subtropical jet (STJ) and polar front jet (PFJ) during ENSO events. Trenberth (1984) noted reversals in the strength of the PFJ and the STJ during the 1970s with no mention of ENSO correlations. Karoly (1989) demonstrated that there are significant increases of the STJ and decreases of the PFJ over the South Pacific Ocean using seasonal analysis for three composite ENSO warm events from 1972 to 1983. Recently, Kitoh (1994) indicated that the interannual variations of the split jet over the South Pacific Ocean are highly correlated with the SST anomalies in the central equatorial Pacific as well as with the transient and stationary eddy activity.

An analysis of the time series of 300-hPa zonal winds over the South Pacific clearly shows an oscillation in the STJ and PFJ strengths (Fig. 1). Figure 1 contains annual running means averaged over the region from 120°W to the date line (defined here as the South Pacific sector). The analysis is a composite of monthly means from the ECMWF/WMO (European Centre for Medium-Range Weather Forecasts/World Meteorological Organization) analyses from 1980 to 1989 and the ECMWF/TOGA (Tropical Ocean Global Atmosphere) analyses from 1985 to 1994. When the running mean zonal winds are plotted next to the annual running mean SOI, a clear relationship between the phase of the Southern Oscillation and the split jet is apparent. Notably, the STJ is strongest when the SOI is negative (ENSO warm phase) and weakest when the SOI is positive (ENSO cold phase). The opposite relationship holds for the PFJ. The most intriguing event shown in Fig. 1 is the rapid weakening of the STJ and corresponding strengthening of the PFJ associated with the 1989 ENSO cold event. It is this rapid reversal in the STJ–PFJ strength that made the 1986–89 ENSO cycle the focus of this case study.

The subsequent analysis of the 1986–89 ENSO cycle shows 1) the evolution of an oscillation in the split jet over the South Pacific sector, 2) changes over the cycle in other variables related to the split jet oscillation, 3) associated variations in the momentum budget for the South Pacific sector, and 4) the way the split-jet oscillation may relate to high-latitude interannual fluctuations. As a result, the analysis shows that the variations in the split jet are a consequence of the poleward propagation of the ENSO signal.

Note that throughout the article any reference to the minimum is the 1987 SOI minimum, the maximum is the 1989 SOI maximum, and the cycle is the 1986–89 ENSO cycle. Section 2 introduces the data used and its reliability and the analysis techniques. Observations from the 1986–89 cycle are presented in section 3 and in section 4 the momentum budget and momentum transports are analyzed. A synthesis of the results is given and implications for high southern latitudes are discussed in section 5.

2. Data and methods

The phase of the ENSO cycle is often determined using an SOI that measures the magnitude of the SLP oscillation over the tropical South Pacific first described by Walker and Bliss (1932). The research presented here utilizes the Climate Analysis Center (CAC) Tahiti-minus-Darwin SOI, shown for 1986–89 in Fig. 2. The CAC SOI is negative during a warm phase of the ENSO cycle, when tropical SST are above normal, and positive during a cold phase (below normal tropical SST). The SOI was smoothed using a 12-month running mean (solid line in Fig. 2) to locate a single minimum and maximum SOI value associated with the 1987 warm phase and the 1989 cold phase. The 1987 minimum occurred between April and May 1987 and the maximum was located between December 1988 and January 1989. Though the minima and maxima of the SOI do not always correspond exactly to the peak of an ENSO warm or cold phase, the correlation was high for the 1987 minimum and the 1989 maximum (Vincent and Schrage 1994). Furthermore, these extrema are a clear reference for centering means and differences in the ENSO cycle.

How to average climate data to best represent the ENSO cycle has been a topic of recent discussion, especially in light of the prolonged warming of the early 1990s. Prior to the 1982–1983 warm phase, van Loon and Shea (1985, 1987) found the ENSO cycle to have a close association with the annual cycle. Furthermore, Meehl (1987) described the phases of ENSO as belonging to strong or weak annual cycles. With the occurrence of the 1982–1983 warm phase, however, the

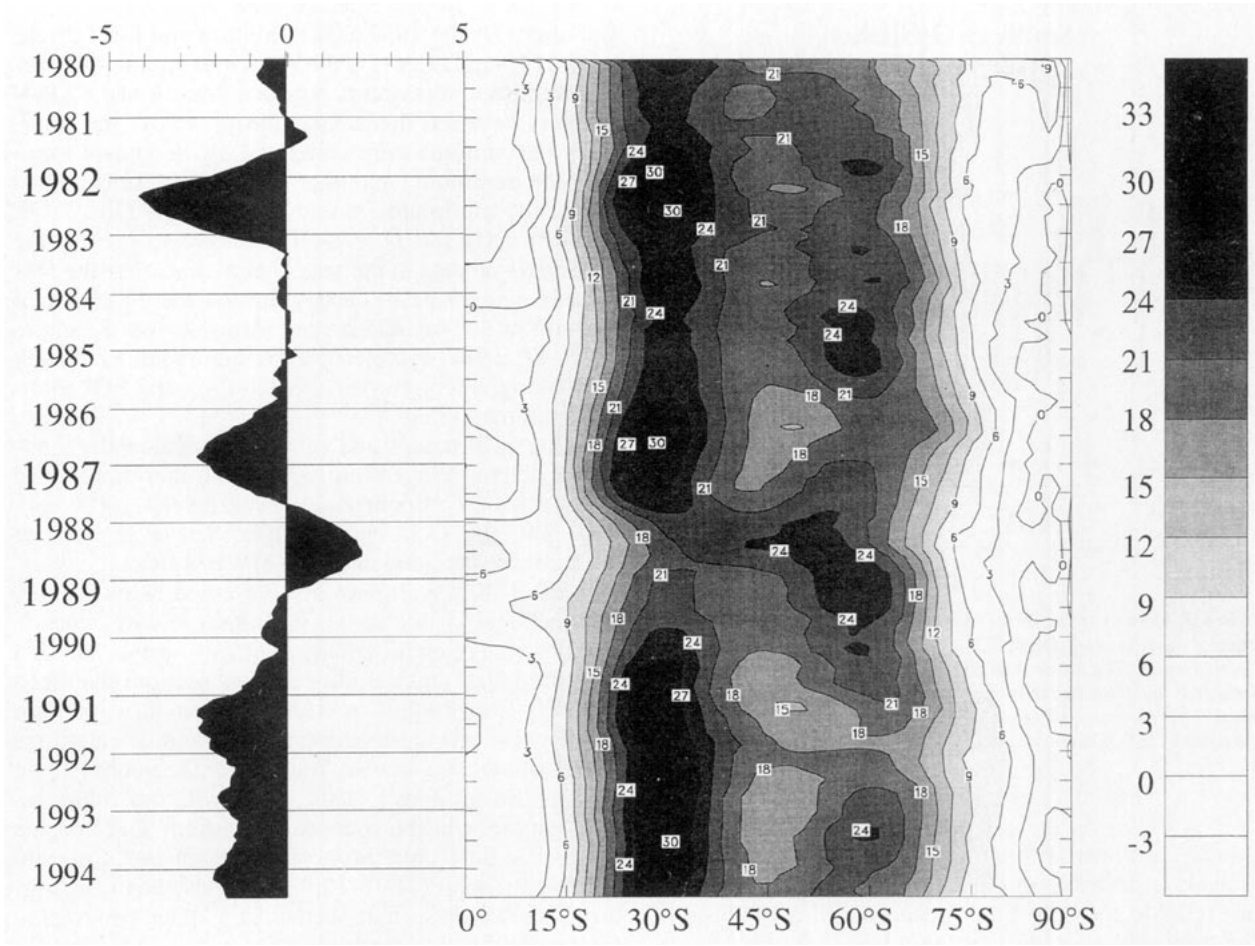

FIG. 1. Annual running mean 300-hPa zonal wind (m s^{-1}) averaged over 120°W–180°. Created by combining the monthly mean ECMWF/WMO (1980–89) analyses and the ECMWF/TOGA (1985–94) analyses. The graph on the left is the annual running mean of the Climate Analysis Center's monthly Tahiti-minus-Darwin Southern Oscillation index (CAC SOI). Calendar years are plotted at the midpoint of each year.

association of ENSO with the annual cycle became less clear (Wang 1992). Wang (1995) described how interdecadal changes can alter the evolution of the ENSO warm and cold phases. With the understanding that variations in the seasonality of ENSO do occur, the interannual variability for the 1986–89 ENSO cycle was focused upon by using annual averages similar to Smith and Stearns (1993), even though annual averages may mask some interesting seasonal circulation anomalies (Karoly 1989).

In an effort to reveal the mechanism that may propagate the ENSO signal poleward, analyses of the entire Southern Hemisphere were needed. The ECMWF/TOGA daily analyses were chosen as the base climate data primarily because the quality of the ECMWF analyses is considered the best among major data centers over the South Pacific Ocean and the high southern latitudes (Sinclair and Cong 1992; Sinclair 1994). The ability of current conventional data collection and analysis schemes to represent the atmospheric conditions over the South Pacific Ocean and higher southern latitudes is a key question in determining the validity of the results to be shown in sections 3 and 4. For this work it is important to find a hemispheric analysis that accurately portrays both the time mean conditions and the eddy components. Genthon and Braun (1995) evaluated six years of previously analyzed surface temperature and predicted precipitation for both Greenland and Antarctica. In spite of sparse conventional observations, they found that the analyzed temperature and precipitation, including seasonality, are in good agreement with satellite observations and previous climatic estimates. Bromwich et al. (1995) intercompared moisture budget calculations from 1985 to 1992 for Antarctica and the Southern Ocean using operational numerical analyses from the Australian Bureau of Meteorology (ABM), the ECMWF/TOGA archive, and the National Meteorological Center (NMC). The results were evaluated against representative rawinsonde sites and indicated that the ECMWF/TOGA analysis (both eddy and mean) overall is much better than the other two datasets, which generally underestimate the trans-

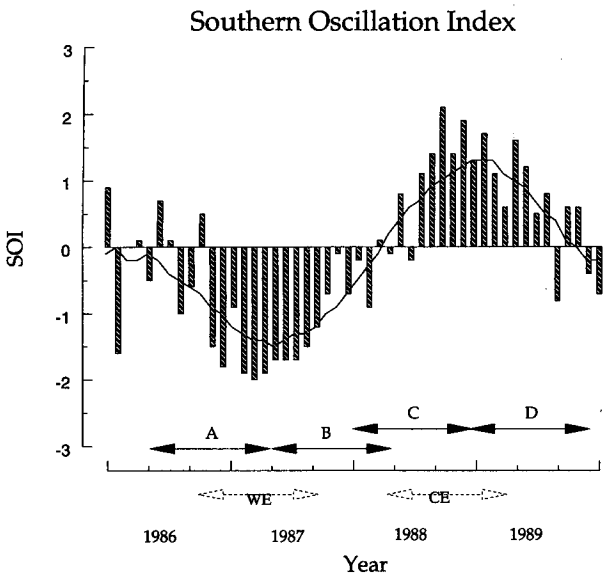

FIG. 2. Monthly mean values of the Southern Oscillation index from January 1986 through December 1989. The solid line is a 12-month running mean. The arrows mark the year before (*A*) and after (*B*) the 1987 SOI minimum and the year before (*C*) and after (*D*) the 1989 SOI maximum. Also marked are the years surrounding the SOI minimum (WE) and the SOI maximum (CE). The SOI is a dimensionless index.

port at each level. From these evaluations and comparisons it is probable that the ECMWF/TOGA analyses are reliable for both time mean and eddy analysis of the troposphere at high southern latitudes.

For the analysis of the observational data, the daily fields were averaged into monthly means. Annual means were then created before and after, and were differenced across, the 1987 SOI minimum and 1989 maximum. The solid arrows on Fig. 2 show the temporal position of annual means for the year before (*A*) and after (*B*) the 1987 SOI minimum and for the year before (*C*) and after (*D*) the 1989 maximum. An overlap of four months occurs between years *B* and *C*. Differences between the annual means across the minimum (maximum) were computed as the annual mean after the minimum (maximum) minus the annual mean before the minimum (maximum), that is, $\mathrm{Dif}_{\min} = B - A$ and $\mathrm{Dif}_{\max} = D - C$. The choice to present the observational data in the years before and after the SOI extrema was made to clearly present the evolution of the split jet stream, and related features, over the entire 1986–89 ENSO cycle. The evolution is not as evident by looking solely at years centered on the SOI minimum and maximum.

The annual means and differences included geopotential height, temperature, and zonal, meridional, and vertical wind components at seven levels: 1000, 850, 700, 500, 300, 200, and 100 hPa. Sea level pressure data are also included in the ECMWF/TOGA analyses. Not all of these variables are presented as only some showed significant changes during the ENSO cycle.

After analyzing all annual averages on the standard pressure levels and meridional cross sections averaged over 60° longitudinal sections around the Southern Hemisphere, the most significant interannual variations in the split jet stream were found over the South Pacific sector (180°–120°W). This, along with our initial interest in the split jet, focused the current study on the South Pacific sector. Some mention of the upstream Australian sector (180°–120°E) will also be made. Figure 3 shows these two sectors and other geographic references made in the text.

Analysis of the momentum budget for the South Pacific sector is used to further investigate the maintenance and changes of the split jet during the 1986–89 ENSO cycle. Calculations are made using the ECMWF/TOGA daily analyses and the following form of the momentum equation:

$$\frac{\partial[\bar{u}]}{\partial t} = f[\bar{v}] - \underbrace{\frac{1}{a\cos^2\phi}\left[\frac{\partial}{\partial\lambda}(g\bar{z}\cos\phi)\right]}_{\mathrm{CT}} - \underbrace{\left\{\frac{1}{a\cos^2\phi}\left(\frac{\partial}{\partial\phi}([\overline{u'v'}]\cos^2\phi) + \left[\frac{\partial}{\partial\lambda}(\overline{u'u'}\cos\phi)\right]\right)\right.}_{\mathrm{CEM}}$$
$$\left. + \left[\frac{\partial\overline{u'\omega'}}{\partial p}\right]\right\} - \underbrace{\left\{\frac{1}{a\cos^2\phi}\left(\frac{\partial}{\partial\phi}([\bar{u}\bar{v}]\cos^2\phi) + \left[\frac{\partial}{\partial\lambda}(\bar{u}\bar{u}\cos\phi)\right]\right) + \left[\frac{\partial\bar{u}\bar{\omega}}{\partial p}\right]\right\}}_{\mathrm{CMM}} + R. \quad (1)$$

Associations between the split-jet oscillation and variations in the ageostrophic circulations, transient eddy activity, the time-mean flow and residual term are illustrated in (1). The standard notation is followed in (1) by dividing each variable into the time mean and its departure, for example, z into

$$z = \bar{z} + z', \quad (2)$$

where the overbar denotes the monthly mean and the prime is the daily departure from the monthly mean. The notation $[z]$ indicates the regional zonal mean of z, that is, from 120°W to 180° for the South Pacific sector, and all terms were calculated at each of the seven pressure levels in the ECMWF/TOGA dataset. In (1) the regional zonal wind tendency is balanced by the Coriolis torque (CT), pressure gradient term (PG),

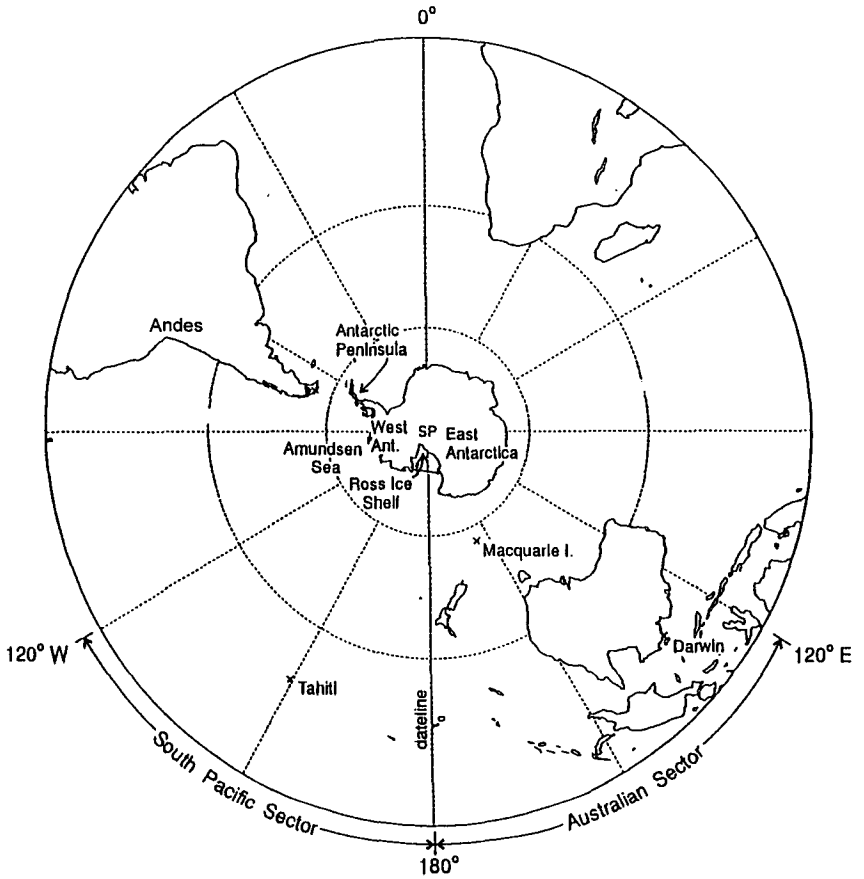

FIG. 3. Location map of the Southern Hemisphere showing the South Pacific and Australian sectors and geographic features referenced in the text. The crosses mark the locations of key surface stations.

three-dimensional transient eddy momentum convergence (CEM), three-dimensional time mean flow momentum convergence (CMM), and residual term (R) that includes friction and observational and computational errors.

To analyze the relationship between eddy activity, on short and long timescales, and the split jet, Lanczos filtering of the ECMWF/TOGA daily analyses was used. Lanczos filtering, a Fourier method of filtering digital data, yields 2.5–6-day bandpassed data (Duchon 1979). Lanczos filtering involves transforming an original input data sequence x_t where t is time, into a filtered output data sequence y_t using the linear relationship

$$y_t = \sum_{k=-n}^{n} w_k x_{t-k}, \tag{3}$$

where the w_k are smoothed weighting functions

$$w_k = \left(\frac{\sin 2\pi f_{c2} k}{\pi k} - \frac{\sin 2\pi f_{c1} k}{\pi k} \right) \frac{\sin \pi k/n}{\pi k/n} \tag{4}$$

and $n = 8$ is the total number of weights; the two cutoff frequencies f_{c1} and f_{c2} correspond to 2.5 and 6 days, respectively. This filter is used to calculate the 2.5–6-day eddy momentum flux to examine the synoptic eddy activity. The difference between the monthly averaged total eddy flux term from (1) and the result of the Lanczos filtering approximates the low-frequency 7–30-day eddy flux.

3. Observations

a. Zonal winds

The split jet is climatologically located over the Australian sector, with its branches often extending into the South Pacific sector (van Loon 1972). In the zonal average, the polar front branch of the jet is primarily forced by the baroclinic eddies (Chen 1994; Trenberth 1991), while the STJ can qualitatively be explained from the conservation of angular momentum (Palmen and Newton 1969) and tropical heating (Hurrell and Vincent 1990, 1991). The role of high southern latitudes in the maintenance of the split in the jet is de-

scribed by James (1988), who showed that the topography and atmospheric temperature structure of Antarctica play a key role. Furthermore, a possible ENSO–Antarctic connection to the split jet was described by Mo et al. (1987). They found that cold air releases from Antarctica were partially responsible for maintaining 500-hPa blocking, and thus a split jet stream, prior to the 1982 ENSO warm phase.

A split flow at 300 hPa is clearly evident, especially in the Australian sector, in the zonal wind component for the year before the 1987 SOI minimum (Fig. 4a). The split is characterized by a strong (>28 m s^{-1}) STJ that extends eastward well into the South Pacific sector along 25°S. The PFJ in the South Pacific sector is much weaker. In the year after the minimum (Fig. 4b), the subtropical branch of the split jet weakens slightly while the PFJ maximum stretches eastward along 50°S and strengthens slightly.

The zonal winds during the year before the 1989 SOI maximum (Fig. 4c) reveal a dramatic decrease in the strength of the subtropical branch of the split jet. Meanwhile, a new jet core is generated at 45°S, 130°W and the PFJ in the Australian sector extends to the South Pacific sector. These indicate the PFJ strengthened over the South Pacific sector. After the maximum, the eastward elongation of the PFJ continued (Fig. 4d) reaching across the tip of South America, while the portion of the PFJ near the date line moved closer to Antarctica

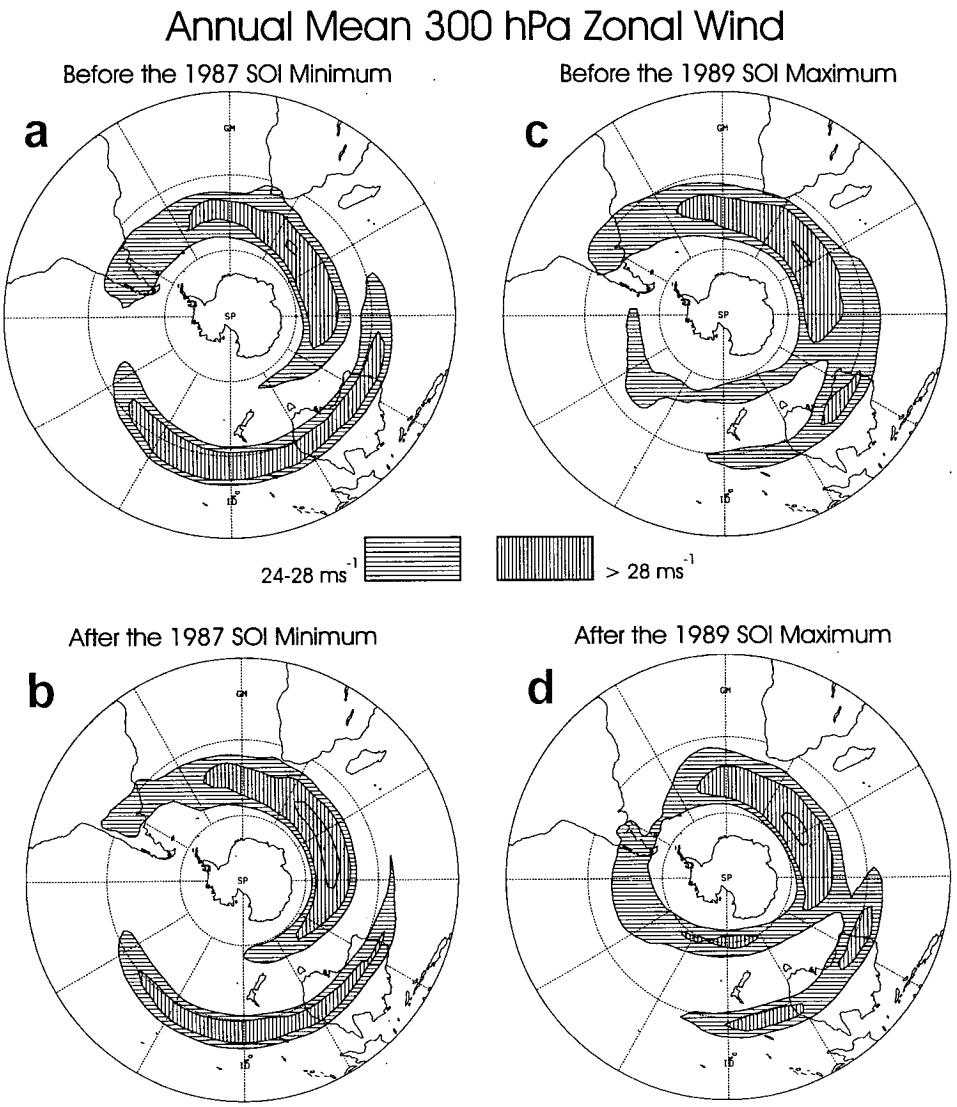

FIG. 4. Annual mean 300-hPa zonal wind component for (a) the year before and (b) the year after the 1987 SOI minimum and (c) the year before and (d) the year after the 1989 SOI maximum. Contours are drawn at 24, 28, and 32 m s^{-1} and the shading is defined in the legend.

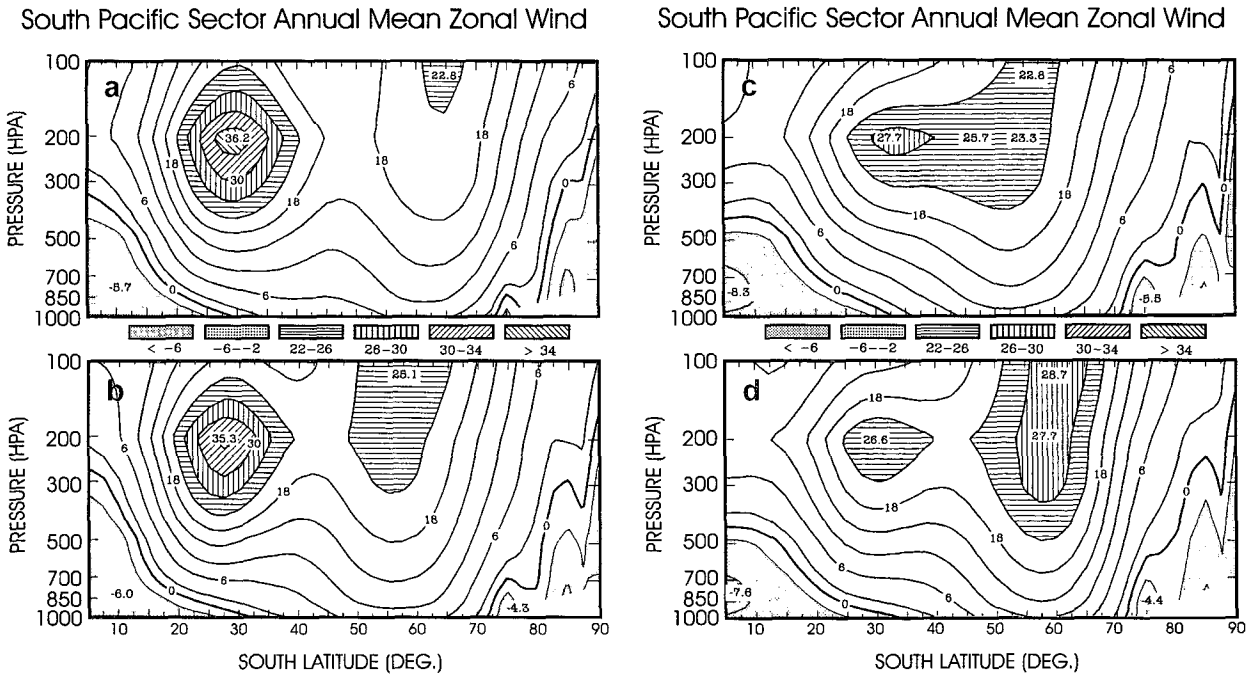

FIG. 5. Meridional cross sections of the zonal wind component averaged over the South Pacific sector for (a) the year before and (b) the year after the 1987 SOI minimum and (c) the year before and (d) the year after the 1989 SOI maximum. Contours are drawn every 4 m s^{-1} starting at ± 2 m s^{-1} with a zero line added for clarity. Westerly jets are shaded using a line fill and easterly jets with a dot fill as noted in the legend. The region coinciding with the topography of Antarctica is blocked out.

and strengthened to over 28 m s^{-1}. In summary, the split jet undergoes a clear reversal in the strength of the STJ and the PFJ during the ENSO cycle. Furthermore, though strength changes occur in the Australian sector, the largest variations of the split jet are within the South Pacific sector.

Analysis of the oscillation in the split jet in the vertical dimension was accomplished using regional zonal mean cross sections for the South Pacific sector (Figs. 5a–d). Before the SOI minimum (Fig. 5a), the STJ was much stronger (36.2 m s^{-1}) than the PFJ (22.8 m s^{-1}), and after the minimum (Fig. 5b), the STJ weakened slightly, while the PFJ started to strengthen reaching 25.1 m s^{-1}. Dramatic changes occurred in the strength of the STJ in the year before the maximum (Fig. 5c) as its core speed dropped 22% to 27.7 m s^{-1}. Meanwhile, the PFJ continued to strengthen though its core became less well defined. After the SOI maximum (Fig. 5d), the STJ weakened further to only 26.6 m s^{-1}, while the PFJ strengthened to 28.7 m s^{-1}. Overall changes in the strength of the jets from before the SOI minimum to after the maximum (*A* to *D*) resulted in a 27% reduction in the STJ and a 26% increase in the PFJ.

b. Geopotential height differences

Individual atmospheric features are hard to define in annual average fields at upper levels so differences across the minimum and maximum were examined. In general, the height differences poleward of 30°S show similar patterns for all levels of the troposphere. Figure 6 shows the 300-hPa level differences that reveal pattern changes consistent with the increase in strength of the PFJ during the cold phase. Over the South Pacific Ocean, a southward drift and strengthening of the positive differences near the date line occurs from the SOI minimum to the maximum. Also the upper-level low over the Amundsen Sea (60°S, 160°W) during the warm phase shifts eastward and deepens during the cold phase. These changes in the height field are consistent with an increase in the geopotential gradient near 60°S during the cold phase and are likely associated with the observed increase in the PFJ strength.

Another interesting feature over the South Pacific is a hook-shaped trough–ridge couplet, clearly visible at all levels and marked on the 300-hPa differences in Fig. 6a. The couplet is likely associated with the active SPCZ, which had a peak in intensity, as shown by heavy precipitation patterns (Arkin and Janowiak 1993), during the warm phase. Recall that other authors have speculated that the SPCZ may propagate the ENSO signal poleward (Vincent 1994). The trough–ridge couplet is not apparent in the differences for the 1989 SOI maximum (Fig. 6b).

c. SLP fields

Moving down in the atmosphere to the surface, interesting features also appear in the SLP analyses (Fig.

7). Looking at the Amundsen Sea low, a deepening occurs throughout the cycle from 983 hPa before the minimum to 975 hPa after the maximum. This is consistent with deepening of the upper-level low over the Amundsen Sea noted in Fig. 6. The SLP analyses also show an increase in the strength of the Southeast Pacific high, from 1019 to 1023 hPa, as the Southern Oscillation changes from the 1987 warm phase to the 1989 cold phase.

The deepening of the Amundsen Sea low is also apparent in the zonal wind cross sections for the South Pacific sector. Figure 5 reveals two branches of the low-level easterlies (LLE) near the surface at 75°S (-2.2 m s^{-1} in Fig. 5a) and 85°S (-9.0 m s^{-1} in Fig. 5a). These respectively correspond to the circulation around the Amundsen Sea low and the katabatic drainage from West Antarctica (Bromwich et al. 1994). While the LLE at 85°S do not change significantly, the 150% increase (from 2.2 to 5.5 m s^{-1}) in the strength of the LLE at 75°S from before the minimum to before the maximum (*A* to *C*) corresponds to the deepening and positioning of the Amundsen Sea low over this period (Fig. 7). However, the strength of the LLE at 75°S weakens to 4.4 m s^{-1} in *D*, in association with an eastward shift in the Amundsen Sea low.

Figure 7a also shows a distinct trough extending equatorward near 150°W that is not present in the other three annual averages. This trough is likely associated with the strong SPCZ during this period. The position of the SPCZ is noted with the bold dotted line in all frames of Fig. 7 and was plotted using the axis of heavy precipitation obtained from Arkin and Janowiak (1993).

4. Momentum budget and eddy transport

To understand the changes in the split jet depicted by the zonal wind analyses, the various terms of the momentum equation (1) were calculated for the South Pacific sector. After ignoring the small tendency term on the annual basis, the momentum equation reduces to

$$R = -(\mathrm{FV}_{ag} + \mathrm{CEM} + \mathrm{CMM}), \qquad (5)$$

where the ageostrophic component (FV_{ag}) is the sum of Coriolis torque (CT) and pressure gradient term (PG) in (1). The leading terms or the signs of them in (5) are expected to be closely associated with the variation of the STJ and PFJ in the upper troposphere. The terms on the right-hand side will not completely balance, especially at lower levels, due to the omission of surface frictional effects. To reduce the huge error over high latitudes induced by the spectrally analyzed ECMWF data (Trenberth 1992), a 200-km zonal running mean was applied to the data before calculating the momentum budget, and linear extrapolation was used to calculate the terms at the pole. These corrections significantly reduce the error in the polar region and have minimal or no effect in middle and low latitudes.

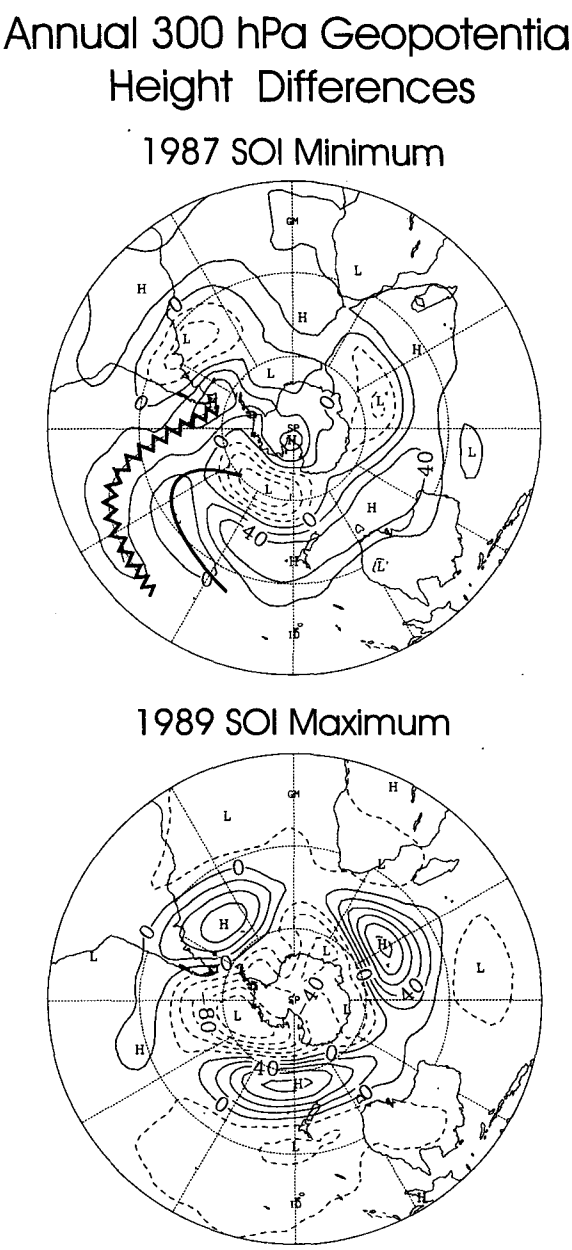

FIG. 6. Annual mean 300-hPa geopotential height differences for (a) the 1987 SOI minimum and (b) the 1989 SOI maximum. The contour intervals are 20 gpm and negative differences dashed. The trough–ridge hook pattern is marked in (a) using standard notation (see text).

a. Vertical cross section of momentum budget

Figure 8 shows the results from (5) for the year before the 1987 SOI minimum, with the "J" marking the cores of the STJ and PFJ. The momentum convergence

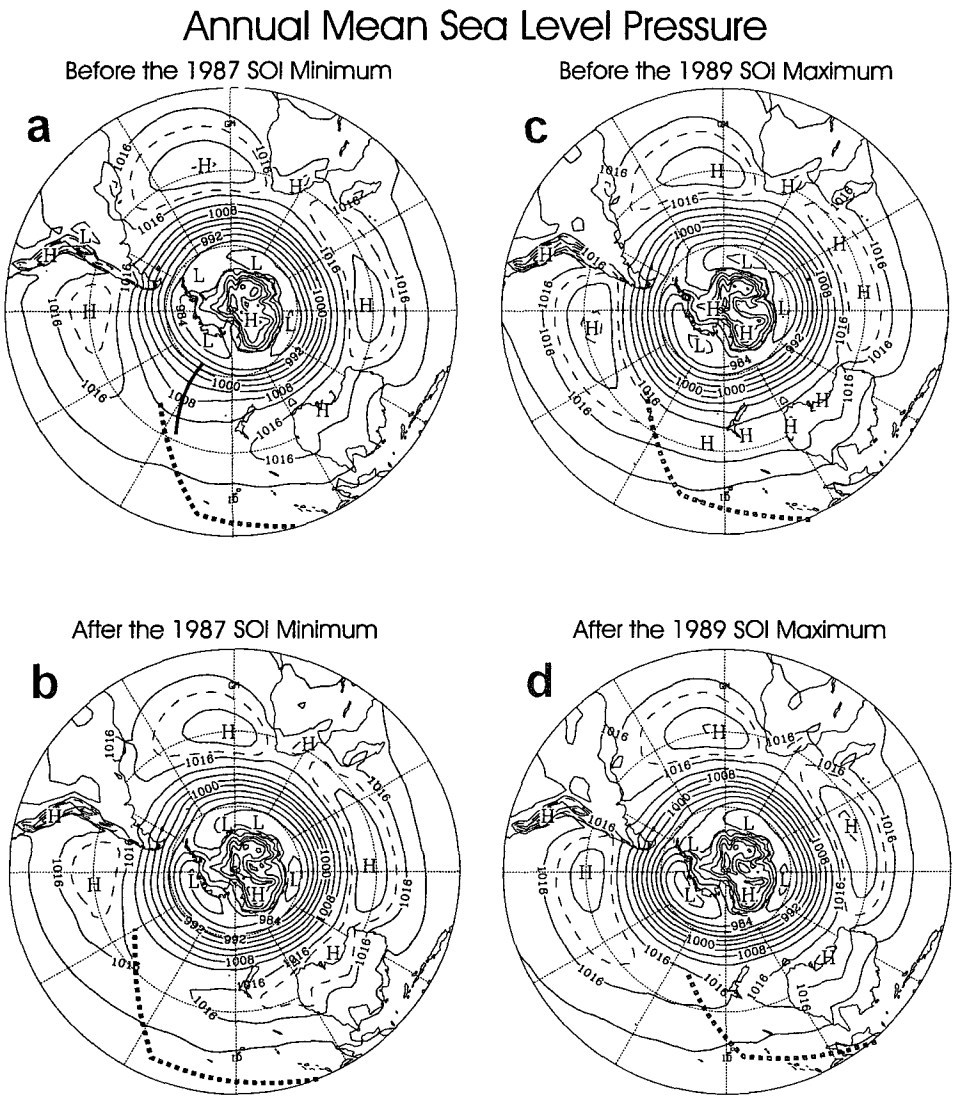

FIG. 7. Annual mean sea level pressure fields for (a) the year before and (b) the year after the 1987 SOI minimum and (c) the year before and (d) the year after the 1989 SOI maximum. Contours are drawn every 4 hPa, with dashed lines at 1018 and 1022 hPa for added clarity at low latitudes. A distinct trough is marked with a bold solid line in (a) and the lines of filled squares mark the axis of maximum precipitation in the SPCZ taken from Arkin and Janowiak (1993). Note that the SLP values over the Antarctic continent and the Andes are questionable due to the high topography.

by the transient eddies (CEM) displays two centers of westerly momentum source in the mid to upper troposphere from 30° to 70°S, with the major maximum near 52°S and a minor maximum at 66°S. The CEM becomes a sink of westerly momentum in the low and midlevels north of 30°S and at all levels poleward of 70°S (Fig. 8a). The momentum convergence of the mean flow (CMM; Fig. 8b) supports the westerlies in the mid- to upper troposphere from 15° to 35°S and poleward of 55°S and slows the westerlies in midlatitudes. The role of the ageostrophic component in jet dynamics is described by Uccellini (1990), and for the first year of the ENSO cycle FV_{ag} acts as a sink of westerly momentum in the upper troposphere from 15° to 35°S and as a source of westerly momentum poleward of 35°S (Fig. 8c). The residual term (Fig. 8d) reflects the dissipation of westerly momentum at the surface in midlatitudes and generation at the surface in low and high latitudes. At tropospheric jet stream levels, the residual indicates that the uncertainty in observation and calculation obscure the small acceleration rate. However, the magnitude of residual in the free atmosphere is less than the leading terms of the momentum equation at most latitudes, except for the area

South Pacific Sector Annual Momentum Budget Before the 1987 SOI Minimum ($\times 10^{-5}$ m s^{-2})

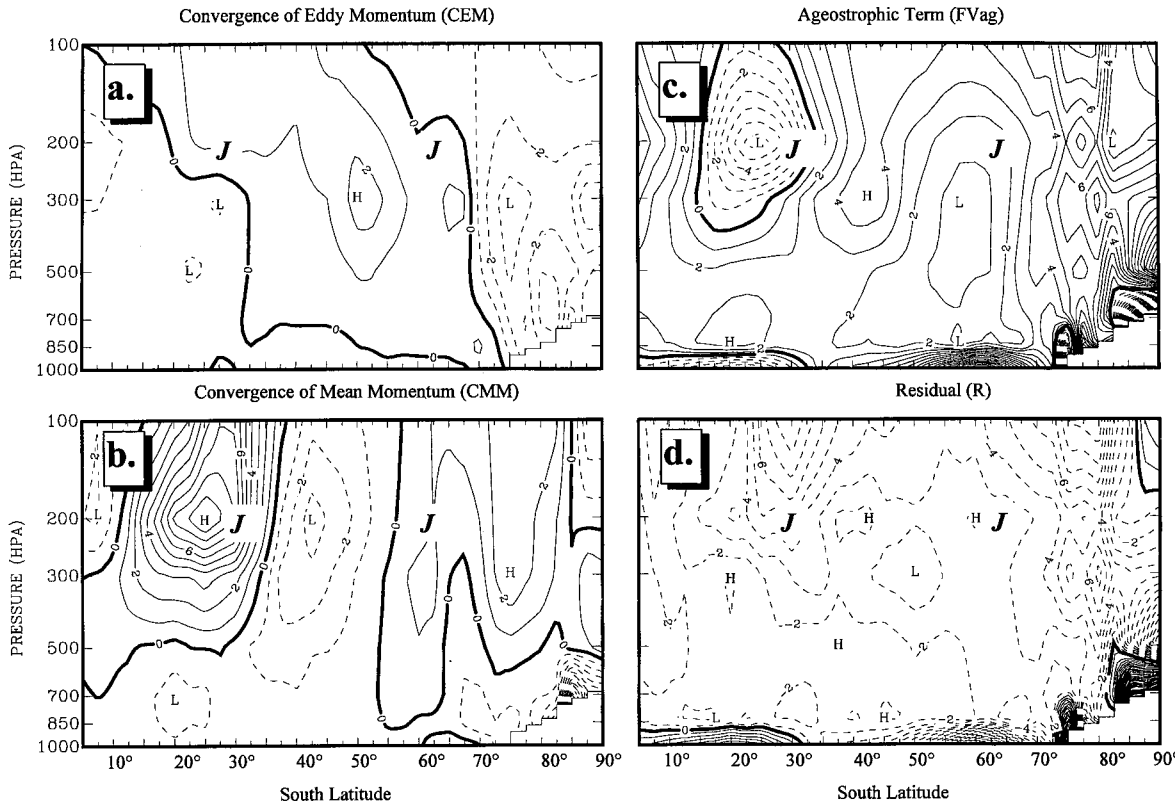

FIG. 8. Annual average cross sections for the South Pacific sector of (a) three-dimensional convergence of eddy momentum (CEM), (b) three-dimensional convergence of mean momentum (CMM), and (c) ageostrophic component (FV_{ag}) computed using momentum equation (1) for the year before the 1987 SOI minimum. The residual term (R) is displayed in (d). Contour interval is 1.0×10^{-5} m s^{-2}. Negative values are dashed and the bold J's mark the cores of the subtropical and polar front jets. Area lying below the surface of Antarctica has been blocked out.

poleward of 80°S. In summary for the year before the minimum, the local STJ was primarily balanced by the westerly momentum source of CMM and the sink of FV_{ag}, whereas the PFJ was mainly supported by the CMM and FV_{ag} with a positive contribution from the eddy activity (CEM).

After the minimum, the changes in CEM and FV_{ag} in Fig. 9 may be associated with the slight increase in strength and equatorward movement of the PFJ and almost no change in the STJ. In the vicinity of the PFJ, CEM increases markedly from 1 to 6×10^{-5} m s^{-2}, while the FV_{ag} changes sign from $+1 \times 10^{-5}$ m s^{-2} to a deceleration of -3×10^{-5} m s^{-2} in response to the increased eddy activity. The location of the CEM center at 55°S corresponds well to the position of the PFJ. Near the core of STJ, a change in the FV_{ag} from -6×10^{-5} to 0×10^{-5} m s^{-2} coupled with more negative forcing from the CEM term and less positive forcing from the CMM contributes to the small change in the STJ strength. It is worth mentioning that the accelerating effect around the STJ from the ageostrophic meridional circulation in year B may reflect the influence of the most active phase of the SPCZ, as well as the eastward movement of its diagonal branch.

The year before the maximum is characterized by large changes in FV_{ag}, which can be associated with dramatic weakening of the STJ (Fig. 5c). The FV_{ag} term (Fig. 10c) showed an enhanced deceleration (from 0 to -4×10^{-5} m s^{-2}) in the region of the STJ core, while the magnitude of the CMM remained near the value in year B. Although the effect of the CEM term on the STJ can be ignored, the northward shift of the PFJ (Fig. 5c) is closely related to the northward shift of the maximum source of westerly momentum in the CEM (Fig. 10a) from 55°S in year B to 50°S. Similar to year B, the westerly momentum contribution to the PFJ is primarily from the CEM.

The momentum budget terms for the year after the 1989 SOI maximum are shown in Fig. 11. The almost unchanged STJ from years C to D may be as-

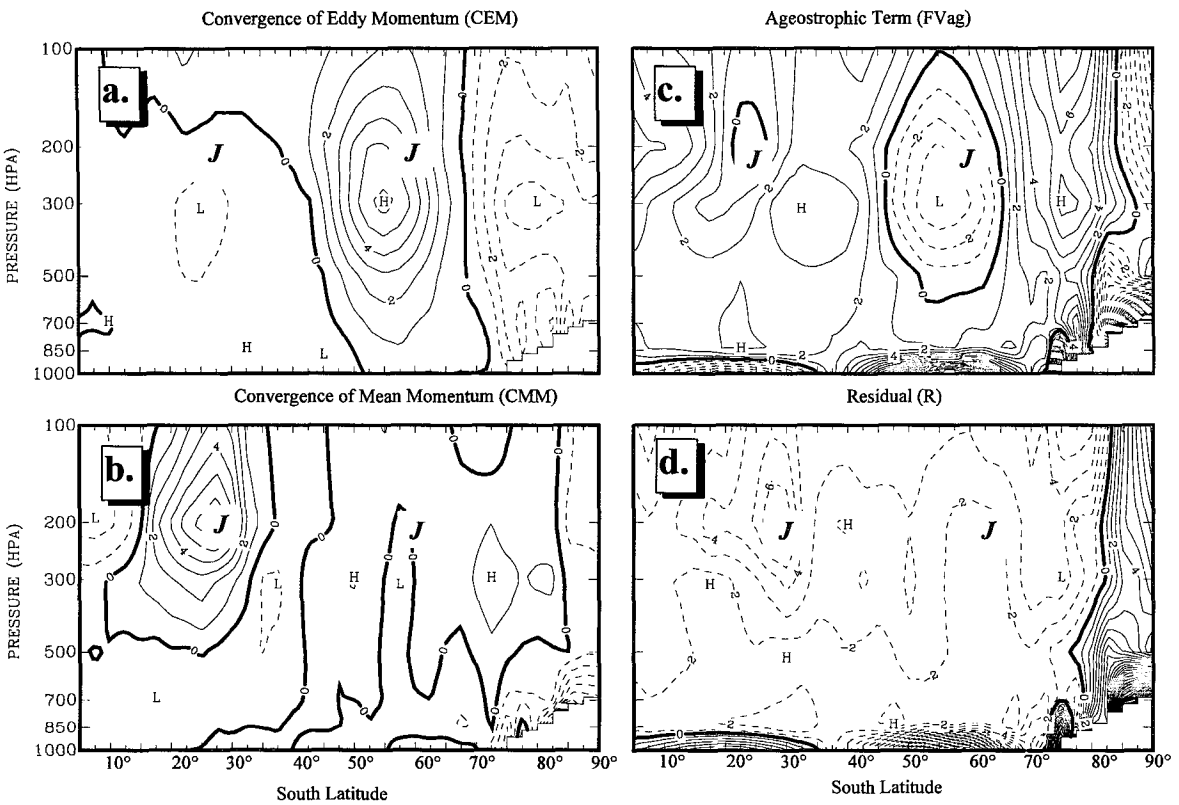

FIG. 9. Same as Fig. 8 except for the year after the 1987 SOI minimum.

sociated with the nearly identical patterns and strength of the leading terms (CMM and FV_{ag}). The most significant difference is that the momentum balance in the vicinity of the PFJ changes from two leading terms to three leading terms. The pattern of the FV_{ag} term (Fig. 11c) is similar to the pattern in year *A*. From years *C* to *D* the maximum shifts poleward from 50° to 60°S and large portions change from a sink to a source of westerly momentum. Meanwhile, the eddy momentum convergence CEM (Fig. 11a) becomes weaker, and the mean momentum convergence CMM, which mainly comes through the lateral boundary with the Australian sector, slightly increases near the core of PFJ in comparison to the previous year.

To further illustrate the relationship of jet variation to momentum budget throughout the ENSO cycle, the anomalies of the residual from the average of years *A*–*D* have been calculated. In the analyses, we assume that the errors and uncertainties in observation and calculation are nearly of the same magnitude and have similar patterns for annual means during the ENSO cycle; in addition, the tendency term and upper-level friction are assumed small enough to be ignored. Because the SOI values for the warm and cold events from 1986 to 1989 are nearly equal in magnitude and duration, the average of years *A*–*D* can be approximately regarded as the mean of a normal year. Under these assumptions, the anomalies of the residual in different phases from its mean for "a normal year" may reveal meaningful changes associated with the jet variations, which are obscured by the errors and uncertainties in the residual term. Figures 12a and 12b show the anomalies of the residual $R_{mean} - R_{warm}$ and $R_{mean} - R_{cold}$ to represent anomalies of westerly momentum residual in the warm phase and cold phase, respectively. During the warm phase, a strong STJ is associated with positive anomalies of westerly momentum residual, while a relatively weak PFJ corresponds with negative anomalies of westerly momentum residual. In the cold phase, a weak STJ is linked to negative anomalies of westerly momentum residual and a strong PFJ fits with positive anomalies of westerly momentum residual. In this respect, the momentum budget is quite well associated with the jet variation.

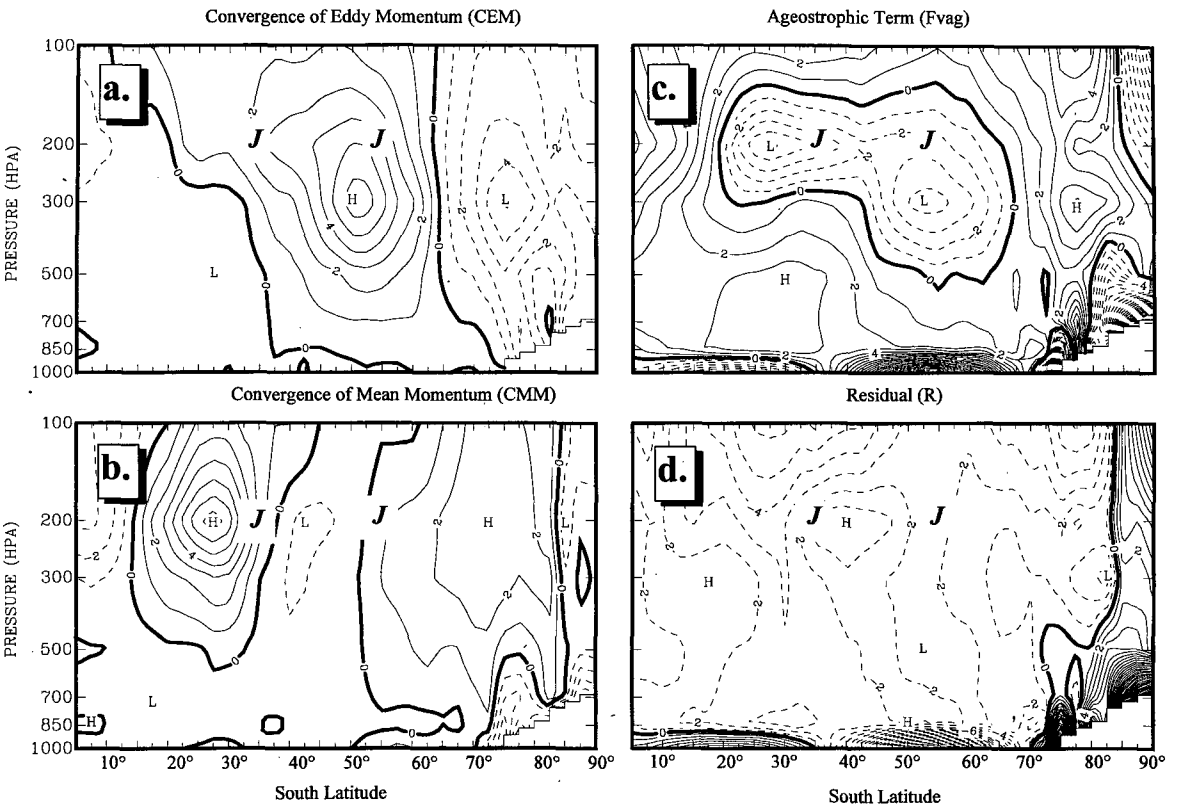

FIG. 10. Same as Fig. 8 except for the year before the 1989 SOI maximum.

b. Temporal variation in momentum analyses at upper levels

The temporal evolution of the PFJ and STJ is clearly displayed using annual running means of the zonal wind averaged for 180°–120°W (Fig. 1). Figure 13a presents a similar analysis focusing on the 1986–89 ENSO cycle. Because the most prominent split jet appears at 200 hPa (Fig. 5), the zonal wind at this level is chosen to analyze jet variations. As expected, the strongest STJ at 200 hPa occurred in early 1987 (summer/fall) while the maximum strength of the PFJ was during the winter of 1989. In the transition period from the warm phase to the cold phase (late 1987 and early 1988), the sudden decrease in the strength of the STJ and the increased magnitude of the PFJ are clearly displayed.

Analysis of the temporal changes in the annual running means of the momentum budget terms identifies how the split-jet oscillation may be related to variations in the values of the terms in (5). The annual running mean momentum budget at 200 hPa (Figs. 13b–d) shows that strengthening of the STJ over the South Pacific Ocean in late 1986 is associated with a strong convergence of mean momentum overwhelming the smaller negative ageostrophic term. The STJ reached its peak intensity in early 1987 when the FV_{ag} term approached zero and the positive values of the CMM term dropped significantly. The minor variations in the CEM term (Fig. 13b) over the subtropics played only a small role in the STJ variations.

Looking more closely at the individual components of the terms in (1) (figure omitted) provided more insight as to the origin of the changes in the STJ. In the CMM term (Fig. 13c), the cross boundary term was the major contributor that may partially be explained by mean flow advection from the upstream Australian sector. For the ageostrophic term (Fig. 13d), the Coriolis term dominated and was associated with the STJ deceleration. This may be a result of the local meridional circulation associated with the diagonal portion of the SPCZ (Vincent 1994), where the warm air rises around 20°S instead of near the equator. The drastic weakening of the STJ in 1988 (early cold phase) is primarily related to an increased negative ageostrophic term during a time when the CMM values remained almost constant from late warm phase to early cold phase.

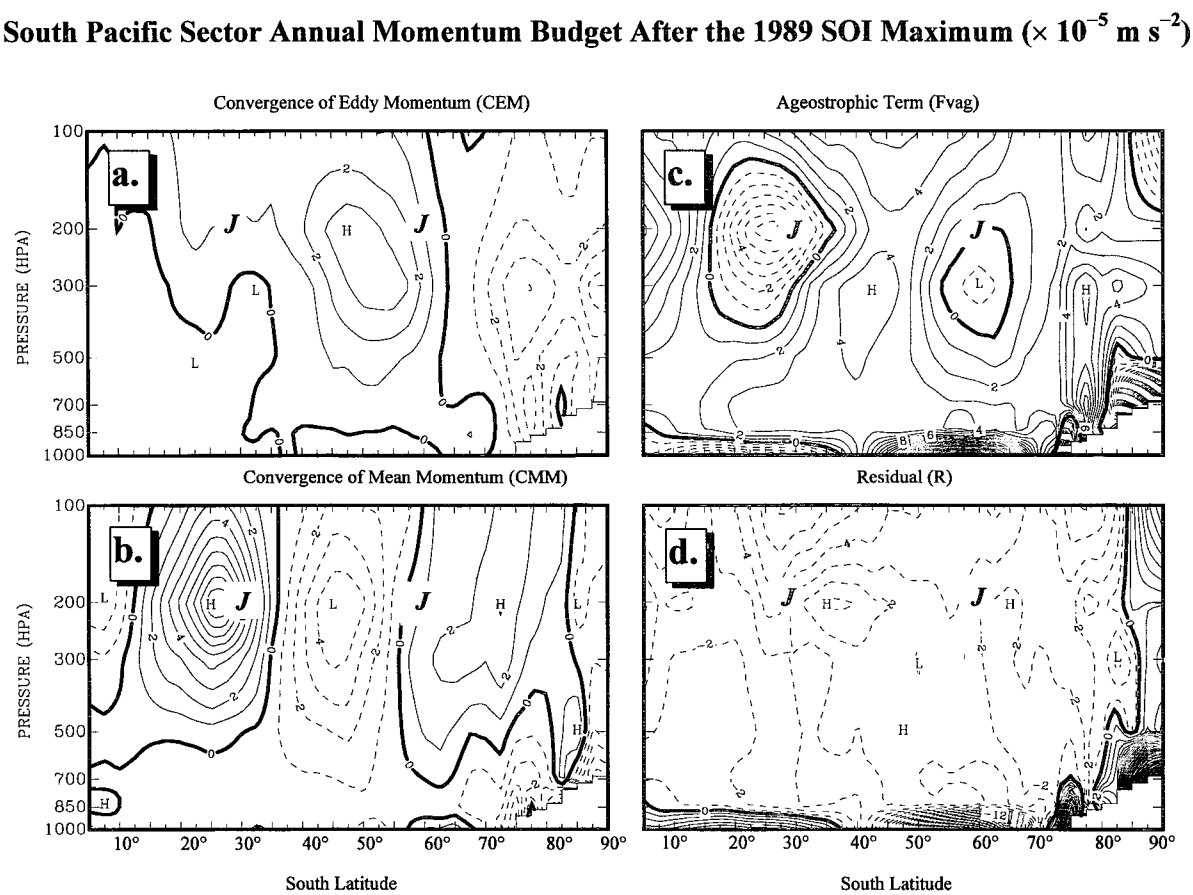

FIG. 11. Same as Fig. 8 except for the year after the 1989 SOI maximum.

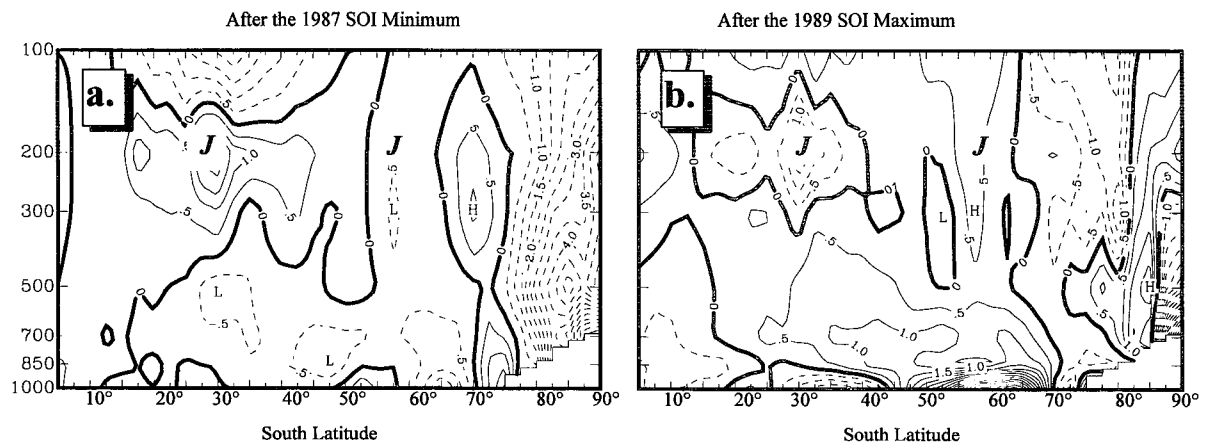

FIG. 12. Anomalies of the residual of momentum budget from the average over the four phases of the ENSO cycle in the South Pacific sector for (a) the year after the 1987 SOI minimum ($R_{mean} - R_{warm}$) and (b) the year after the 1989 SOI maximum ($R_{mean} - R_{cold}$). Contour interval is 0.5×10^{-5} m s^{-2}. Negative values are dashed and the bold J's mark the cores of the subtropical and polar front jets. Area lying below the surface of Antarctica has been blocked out.

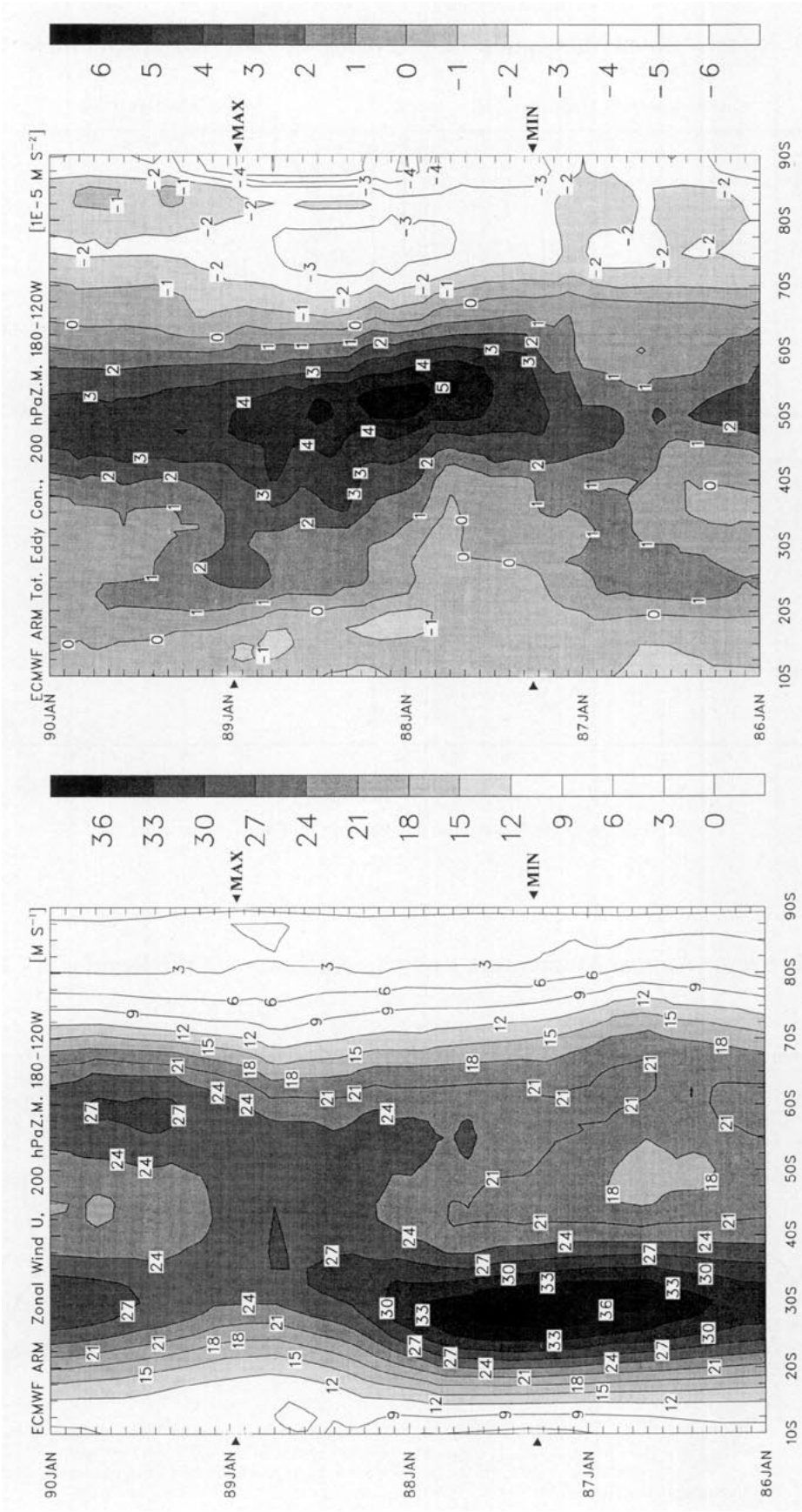

FIG. 13. Hovmöller diagrams of annual running mean (a) zonal wind, (b) CEM, (c) CMM, and (d) FV_{ag} at 200 hPa over the South Pacific sector (120°W–180°) for 1986–89. Triangles mark the position of the SOI minimum and maximum.

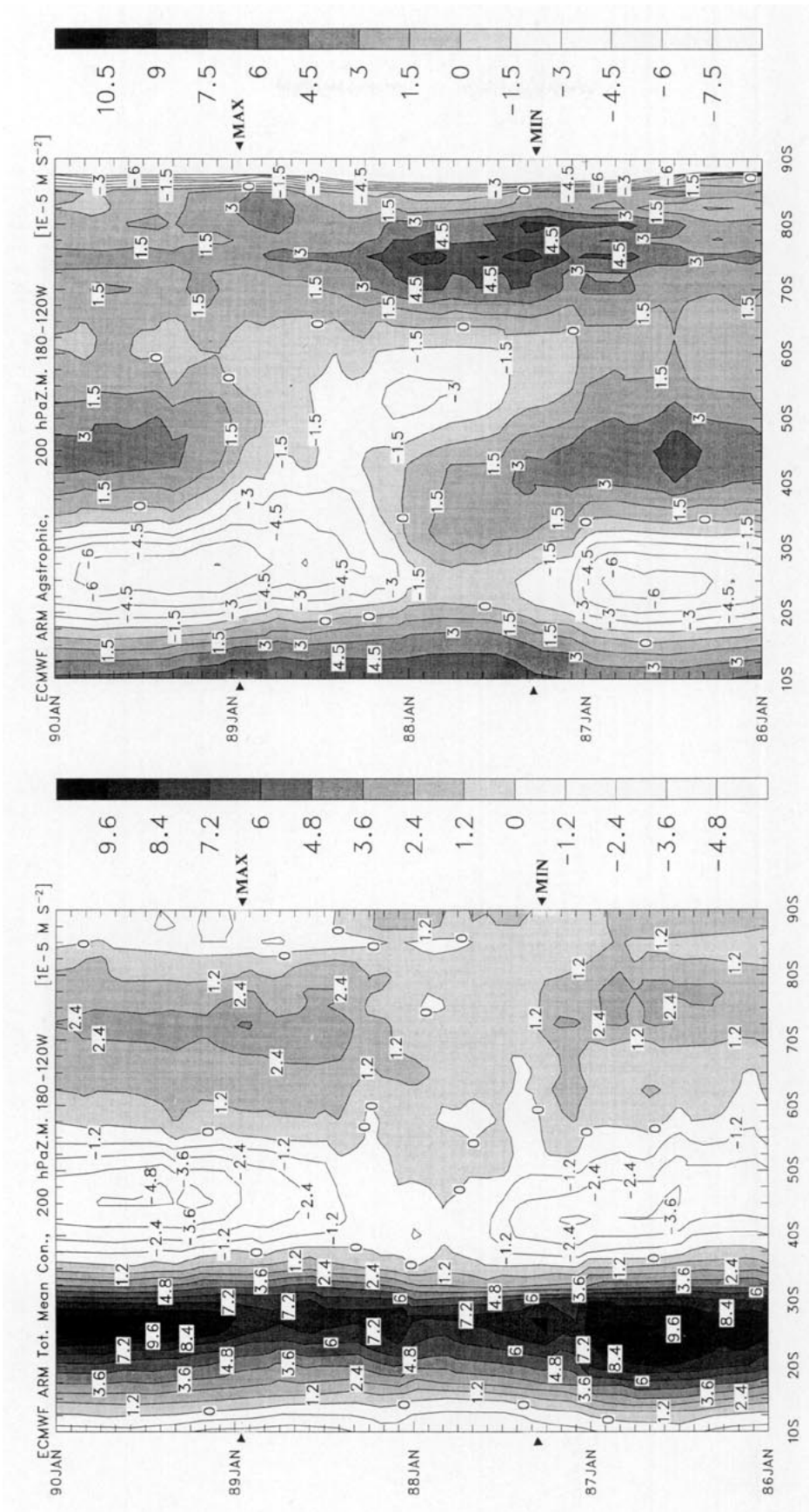

FIG. 13. (*Continued*)

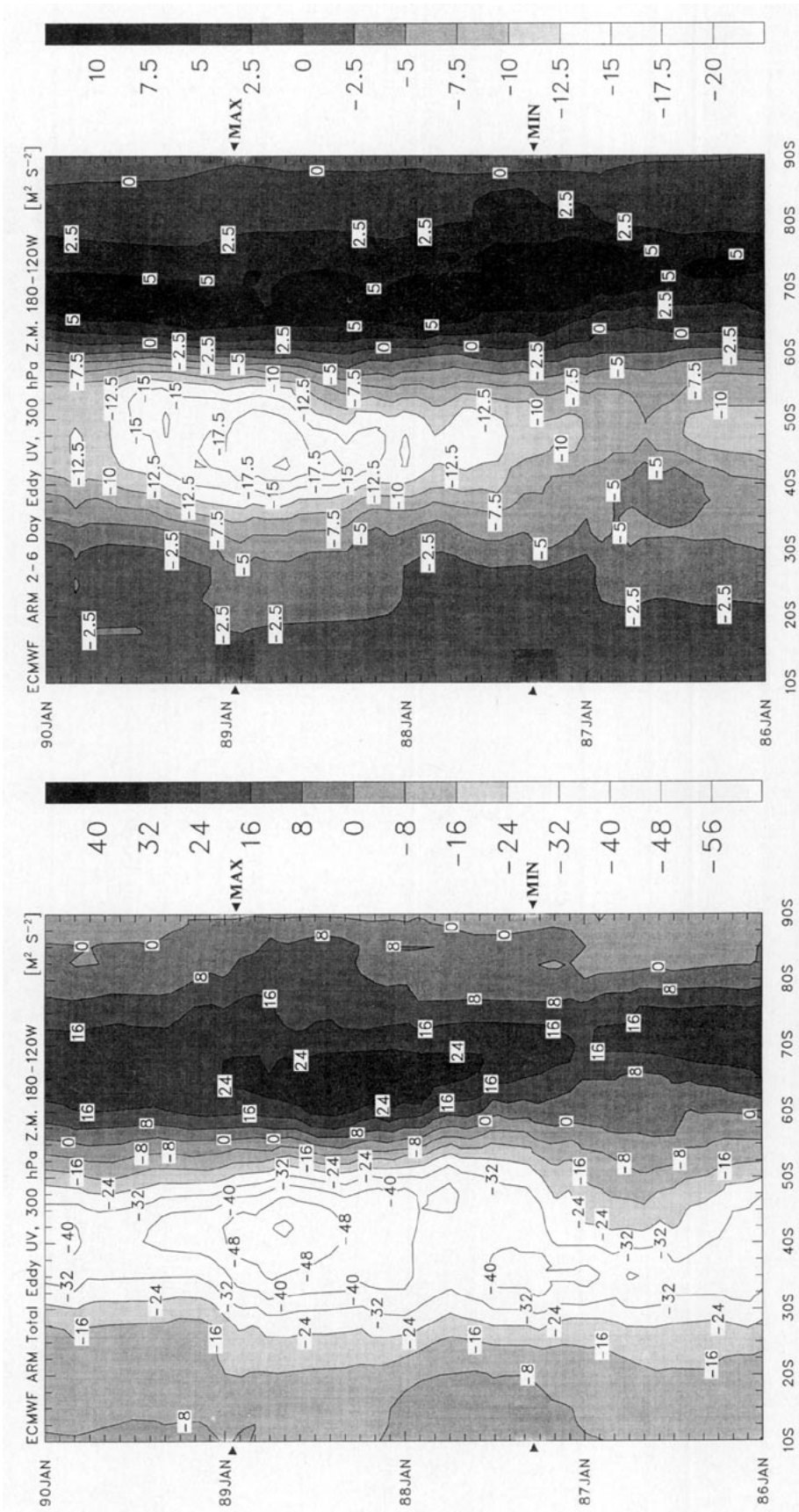

FIG. 14. Hovmöller diagram of annual running mean (a) total, (b) 2.5–6-day, and (c) 7–30-day meridional eddy momentum flux at 300 hPa. Triangles mark the position of the SOI minimum and maximum.

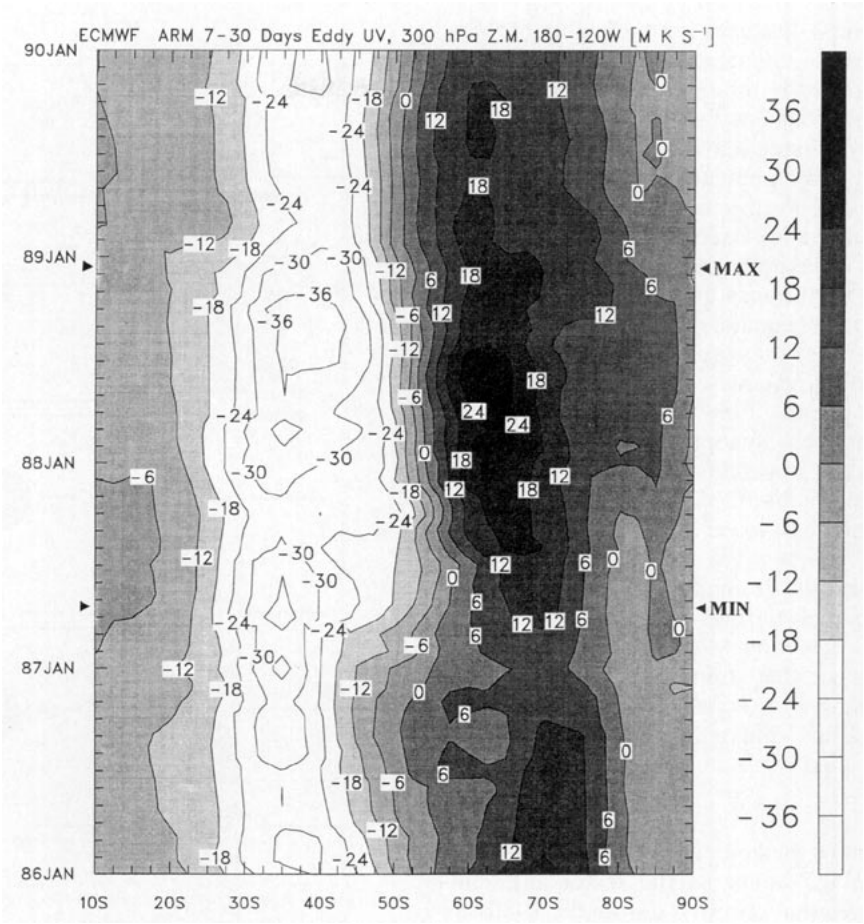

FIG. 14. (*Continued*)

Unlike the STJ, the eddy terms are more strongly associated with changes in the strength of the PFJ over the South Pacific Ocean throughout the ENSO cycle. During the warm–cold phase transition when the PFJ is accelerating, an increasingly negative ageostrophic term (Fig. 13d) developed in response to the drastically increased eddy momentum convergence (Fig. 13b). The ageostrophic response to changes in eddy momentum convergence is the nature of the secondary circulation in the extratropics (Pfeffer 1981; Wu and Chen 1990), with FV_{ag} primarily acting to offset the impacts of eddy activity and being a secondary factor in the wave–mean flow interaction. Note that the CMM term varies only slightly in the region of the PFJ; however, when looking at the individual components of (1), the cross-boundary flow from the Australian sector is important in maintaining the PFJ during 1989.

Now the eddy forcing on the PFJ in the transition period from warm phase to cold phase (or from the STJ dominant stage to the PFJ being prominent) will be further explored. Because the meridional component of the eddy momentum convergence is the key factor in strengthening the PFJ and eddy activity has a maximum at 300 hPa, analyses of meridional eddy momentum fluxes at 300 hPa (Fig. 14a) were created to show how the eddy momentum is actually transported around the PFJ. In general, the maximum convergence of eddy momentum (Fig. 13b) occurs approximately at the zero line of momentum flux (Fig. 14a), suggesting that the poleward transport from midlatitudes and equatorward transport from high latitudes are equally important, although the poleward transport is usually double the equatorward transport. As the cycle oscillates from the warm phase to the cold phase, a clear increase in the momentum transports from both lower and higher latitudes occurs. This phenomenon continues until the beginning of 1989 when the transports begin to decrease. By examining the timing of the poleward and equatorward transport and comparing the transports with eddy momentum convergence at 300 hPa (figure not shown), the strongest convergence of eddy momentum flux that appeared in early 1988 (early cold phase) is contributed to by both the equatorward and poleward eddy momentum transport, with the enhanced equatorward eddy fluxes from high latitudes occurring first.

To identify the time scale of eddy activity related to the changes of the PFJ, a 2.5–6-day bandpass filter,

described in section 2, has been used to obtain the synoptic timescale eddy momentum flux. Figure 14b shows the synoptic eddy momentum flux, while Fig. 14c shows the low-frequency (7–30 day) eddy flux. The synoptic eddy momentum flux at 300 hPa is about 5%–40% of total eddy momentum flux depending on the latitude and time. Furthermore, the poleward synoptic eddy momentum flux has a clear interannual variation that reaches a maximum, about 40% of total poleward eddy momentum transport, around the SOI maximum. Meanwhile, the equatorward synoptic eddy flux from high latitudes has no significant interannual variation, but the lower-frequency eddies maximize their equatorward flux in early 1988. This indicates that the momentum fluxes from synoptic systems (or higher frequency eddies) at upper levels over the high latitudes of the South Pacific Ocean show less signature from ENSO events than lower-frequency eddies. The intensification of equatorward transport of eddy momentum clearly results from the lower-frequency or planetary-scale eddies during the onset of the cold phase (Fig. 14c). In summary, the enhanced eddy momentum convergence that strengthens the PFJ during the cold phase results from equatorward low-frequency eddy momentum flux and poleward high-frequency eddy momentum flux.

5. Synthesis

Figure 15 displays the key elements of the meridional circulation of the South Pacific sector and summarizes the changes that occurred during the 1986–89 ENSO cycle. The primary feature is the split jet. The schematic represents the oscillation in the jet strengths by varying the size of the circles used for the STJ and the PFJ. Note the clear change from a strong STJ and weak PFJ during the warm phase (Figs. 15a,b) to a weak STJ and strong PFJ during the cold phase (Figs. 15c,d). Also shown are the strength of the diagonal portion of the SPCZ diagnosed from precipitation data (Arkin and Janowiak 1993), the deepening of the Amundsen Sea low from the beginning to the end of the cycle, and variations in the twin branches of the Antarctic low-level easterlies (LLE).

The momentum budget calculations imply that the balance between the momentum convergence from the mean flow and the ageostrophic term determines the variation of the STJ. Figure 16 summarizes the findings of the momentum calculations for the South Pacific and Australian sectors for the year surrounding the SOI minimum and maximum, the WE and CE, respectively, in Fig. 2. From WE to CE, the decrease in the strength of the STJ in the South Pacific sector (S_s) is associated with a decrease in the CMM term, while there is only a small change in the ageostrophic term. Note that little change occurs in the CEM in the South Pacific sector and thus the role of eddies in the STJ evolution is small.

Changes in the PFJ in the South Pacific sector, however, appear to be closely linked to variations in the

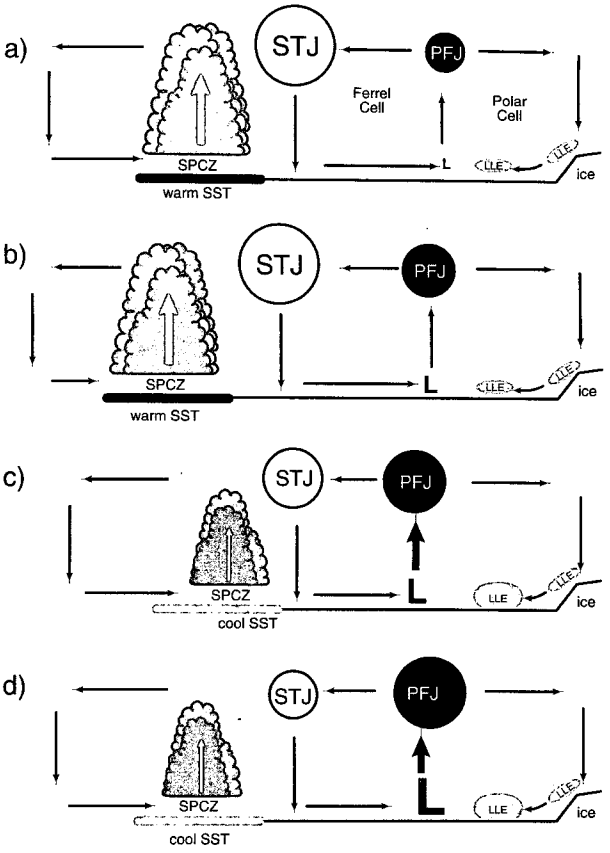

FIG. 15. Schematic meridional cross sections for the South Pacific sector for (a) the year before and (b) the year after the 1987 SOI minimum and (c) the year before and (d) the year after the 1989 SOI maximum. The size of the clouds represents the strength of the South Pacific convergence zone (SPCZ) and the size of the circles represent the strength of the subtropical (STJ), polar front (PFJ), and low-level easterly (LLE) jets. The size of the "L" represents the strength of the Amundsen Sea low.

eddy activity. Figure 16 shows that in the region of the PFJ (S_p) little change in the FV_{ag} term occurs from the WE to the CE, and the slightly more negative CMM term likely results from cross boundary mean flow. An increase in the CEM near the PFJ during the cold event is quite apparent (Fig. 14) and, as denoted by the darker arrows, results from an increase in poleward synoptic eddy momentum flux and equatorward 7–30-day eddy momentum flux. Though we can only speculate as to the source of the increased poleward cyclonic activity, two main sources are probable: the storm track from south of Australia (Streten and Troup 1973; Trenberth 1991; Kitoh 1994) and storms of subtropical origin leaving the southwestward shifted SPCZ (Vincent 1985).

The increase in eddy activity at high latitudes is apparent in the SLP analyses as the Amundsen Sea low deepens significantly in the cold phase. Shiotani (1990) showed that at seasonal scales when the height in the

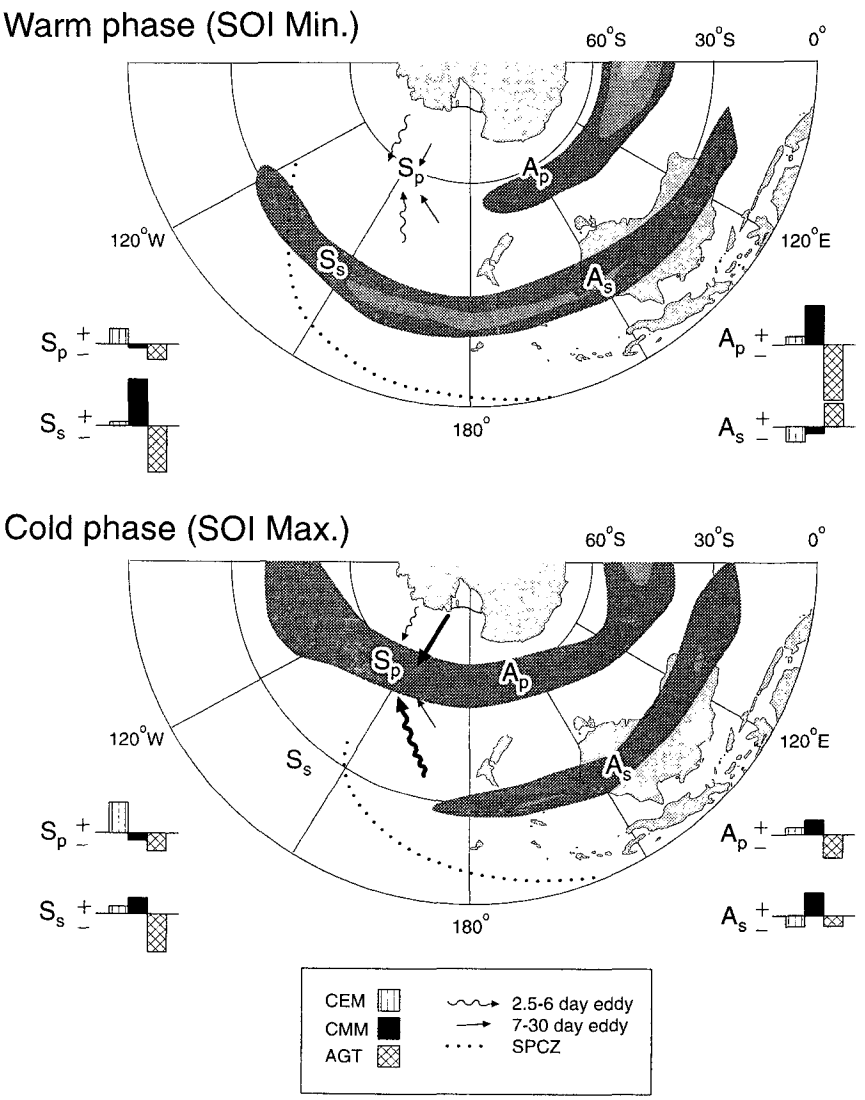

FIG. 16. Schematic representation of changes at 300 hPa in the terms of the momentum equation (see text) for (a) the SOI minimum (WE) and (b) the SOI maximum (CE). The small graphs show the relative magnitudes of the CEM, CMM, and FV_{ag} terms as denoted by the legends for the STJ in the South Pacific sector (S_s) and the Australian sector (A_s) and for the PFJ, S_p, and A_p, respectively. The arrows near S_p represent the magnitudes of the 2–6.5-day and the 7–30-day meridional eddy momentum fluxes. The dotted line marks the average position of the SPCZ during each time period.

polar region is low and the split jet is prominent, transient eddy activity along Antarctica is vigorous in the vicinity of the Ross Ice Shelf and maintains the PFJ. On the other hand, the equatorward transport of eddy momentum from Antarctica may be associated with the maintenance of the boundary layer drainage flow over the continent (Egger 1985; James 1989; Parish and Bromwich 1991). To understand the angular momentum balance associated with the katabatic wind circulation over Antarctica, James (1989) suggested a number of mechanisms to achieve the necessary northward flux of westerly momentum, which included the effects of decaying midlatitude weather systems. Egger (1992) and Detten and Egger (1994) showed that synoptic-scale waves propagating around Antarctica are modified by the Antarctic topography such that westerly momentum is transported out of the continent.

The increase in the 7–30-day equatorward eddy momentum flux rather than in higher frequencies during the cold phase may in part be explained by the Rossby wave tracing theorem on the sphere (Hoskins and Karoly 1981). The turning latitude, where the shortwaves

(zonal wavenumbers greater than three) from the mid- or high latitudes will be reflected back, is about 60°, so the planetary-scale waves (or lower-frequency eddies) are more active than the short waves (high-frequency eddies) as they propagate from the polar region to lower latitudes. Another possible mechanism is high-latitude blocking anomalies in 1988 (Bromwich et al. 1993) that may enhance the momentum transport on planetary scales.

In contrast to the South Pacific sector, the variation and maintenance of jet streams over the Australian sector is quite different. In general, the strength and position of both jets do not change much, although the mechanism of maintenance in the STJ varies as the WE evolves to the CE. The STJ (A_s) is associated with a positive ageostrophic meridional circulation and a slightly weaker eddy momentum divergence (wave–stress) in the WE with a small contribution from mean momentum divergence; this is similar to the zonally averaged case. This indicates that in the WE the STJ over the Australian sector is enhanced by the local Hadley circulation and advected to the South Pacific sector. However, in the CE, the CMM becomes dominant and switches signs with FV_{ag}, that is, the acceleration from the mean momentum convergence now is balanced by decelerations from the ageostrophic term and eddy stress. On the other hand, the PFJ in the Australian sector (A_p) is mainly associated with mean momentum convergence across the lateral boundary and a strongly negative ageostrophic term. Unlike the case in the South Pacific sector, the eddy forcing is quite small. These results suggest that ENSO impacts and responses vary between sectors.

The increase in eddy activity and the subsequent deepening of the Amundsen Sea low can further explain the increase in the strength of the northern branch of the LLE as the WE evolves into the CE. As was shown in modeling studies by Hines et al. (1995), a deeper Amundsen Sea low results in stronger winds parallel to the West Antarctic coast due to the stronger pressure gradient. The LLE are further enhanced by a barrier wind effect as the northerly winds on the east side of the Amundsen Sea low are deflected by the Antarctic topography. Though not particularly important to the analysis of the upper-level split jet evolution, this discussion of the LLE is included to show consistency at all levels in our analysis of the meridional circulation within the South Pacific sector.

Although the results found here may only apply to the 1986–1989 ENSO cycle, similarities with the work of Trenberth (1984), Meehl (1987), and Karoly (1989) make that unlikely. However, the anomalies in circulation and momentum budget found in this case study might have been mixed with other natural variations. To further explore the relationship and mechanism between the ENSO and southern high-latitude circulation, split jet structures over many SOI minima and maxima (normal) will need to be composited. At high latitudes, this work shows that changes in the Southern Oscillation, and thus changes in the phase of ENSO, result in significant changes in the weather of the Amundsen Sea, West Antarctica, and the Ross Ice Shelf. These high latitude changes are probably responsible for interannual variations of precipitation over the West Antarctica ice sheet (Bromwich et al. 1995), and understanding of these changes is necessary for identifying the ENSO signal in the long-term ice record. The variations found in the strength of the high latitude meridional circulation of the South Pacific sector may also be in part responsible for interannual variations in sea ice cover and seal populations as described by Simmonds and Jacka (1995), Gloersen (1995), and Testa et al. (1991).

In conclusion, these results suggest that the variations in the split jet reflect the poleward propagation of the ENSO signal via the South Pacific convergence zone. In the future, it would be desirable to explore the origin of eddy activity changes and to relate the Pacific South American pattern (Karoly 1989; Kitoh 1994) and the SPCZ (Vincent 1994) to the PFJ behavior.

Acknowledgments. We appreciate extensive discussions with Dayton Vincent. Constructive comments from David Karoly and an anonymous reviewer substantially improved the article. Special thanks go to Xuguang Pan for her computational efforts. Beth Daye and John Nagy did exemplary work with the graphics. The ECMWF analyses were obtained from the National Center for Atmospheric Research. This research was funded by the National Science Foundation, Office of Polar Programs Grant OPP-9218949 to David H. Bromwich.

REFERENCES

Arkin, P. A., and J. E. Janowiak, 1993: Tropical and subtropical precipitation. *Atlas of Satellite Observations Related to Global Change,* R. J. Gurney, J. L. Foster, and C. L. Parkinson, Eds., Cambridge, 165–180.

Bromwich, D. H., J. F. Carrasco, Z. Liu, and R.-Y. Tzeng, 1993: Hemispheric atmospheric variations and oceanographic impacts associated with katabatic surges across the Ross Ice Shelf, Antarctica. *J. Geophys. Res.,* **98(D7),** 13 045–13 062.

——, Y. Du, and T. R. Parish, 1994: Numerical simulation of winter katabatic winds from West Antarctica crossing Siple Coast and the Ross Ice Shelf. *Mon. Wea. Rev.,* **122,** 1417–1435.

——, F. M. Robasky, R. I. Cullather, and M. L. Van Woert, 1995: The atmospheric hydrologic cycle over the Southern Ocean and Antarctica from operational numerical analyses. *Mon. Wea. Rev.,* **123,** 3518–3538.

Carleton, A. M., 1988: Sea ice–atmosphere signal of the Southern Oscillation in the Weddell Sea, Antarctica. *J. Climate,* **1,** 379–388.

Chen, B., 1994: Double jets and storm tracks in a two-level primitive equation model of the atmosphere. Ph.D. thesis, Texas A&M University, 131 pp.

Detten, Y., and J. Egger, 1994: Topographic wave modification and the angular momentum balance of the Antarctic troposphere. Part II: Baroclinic flows. *J. Atmos. Sci.,* **51,** 3351–3359.

Duchon, C. E., 1979: Lanczos filtering in one and two dimensions. *J. Appl. Meteor.,* **18,** 1016–1022.

Egger, J., 1985: Slope winds and the axisymmetric circulation over Antarctica. *J. Atmos. Sci.,* **42,** 1859–1867.
——, 1992: Topographic wave modification and the angular momentum balance of the Antarctic troposphere. *J. Atmos. Sci.,* **49,** 327–334.
Genthon, C., and A. Braun, 1995: ECMWF analyses and predictions of the surface climate of Greenland and Antarctica. *J. Climate,* **8,** 2324–2332.
Gloersen, P., 1995: Modulation of hemispheric sea-ice cover by ENSO events. *Nature,* **373,** 503–506.
Held, I. M., S. W. Lyons, and S. Nigam, 1989: Transients and the extratropical response to El Niño. *J. Atmos. Sci.,* **46,** 163–174.
Hines, K. M., D. H. Bromwich, and T. R. Parish, 1995: A mesoscale modeling study of the atmospheric circulation of high southern latitudes. *Mon. Wea. Rev.,* **123,** 1146–1165.
Hoerling, M. P., and M. Ting, 1994: Organization of extratropical transients during El Niño. *J. Climate,* **7,** 745–766.
Horel, J. D., and J. M. Wallace, 1981: Planetary scale atmospheric phenomena associated with the Southern Oscillation. *Mon. Wea. Rev.,* **109,** 813–823.
Hoskins, B. J., and D. J. Karoly, 1981: The steady linear response of a spherical atmosphere to thermal and orographic forcing. *J. Atmos. Sci.,* **38,** 1179–1196.
Hurrell, J. W., and D. G. Vincent, 1990: Relationships between tropical heating and subtropical westerly maxima in the Southern Hemisphere during SOP-1, FGGE. *J. Climate,* **3,** 751–768.
——, and ——, 1991: On the maintenance of short-term subtropical wind maxima in the Southern Hemisphere during SOP-1, FGGE. *J. Climate,* **4,** 1009–1022.
James, I. N., 1988: On the forcing of planetary-scale Rossby waves by Antarctica. *Quart. J. Roy. Meteor. Soc.,* **114,** 619–637.
——, 1989: The Antarctic drainage flow: Implications for hemispheric flow on the Southern Hemisphere. *Antarct. Sci.,* **1,** 279–290.
Karoly, D. J., 1989: Southern Hemisphere circulation features associated with El Niño–Southern Oscillation events. *J. Climate,* **2,** 1239–1252.
Kitoh, A., 1994: Tropical influence on the South Pacific double jet variability. *Proc. NIPR Symp. Polar Meteorol. Glaciol.,* **8,** 34–45.
Meehl, G. A., 1987: The annual cycle and interannual variability in the tropical Pacific and Indian Ocean regions. *Mon. Wea. Rev.,* **115,** 27–50.
Mo, K. C., and G. H. White, 1985: Teleconnections in the Southern Hemisphere. *Mon. Wea. Rev.,* **113,** 22–37.
——, J. Pfaendtner, and E. Kalnay, 1987: A GCM study on the maintenance of the June 1982 blocking in the Southern Hemisphere. *J. Atmos. Sci.,* **44,** 1123–1142.
Palmen, E., and C. W. Newton, 1969: *Atmospheric Circulation Systems.* Academic Press, 603 pp.
Parish, T. R., and D. H. Bromwich, 1991: Continental-scale simulation of the Antarctic katabatic wind regime. *J. Climate,* **4,** 136–146.
Pfeffer, R. L., 1981: Wave–mean flow interactions in the atmosphere, *J. Atmos. Sci.,* **38,** 1340–1359.
Philander, S. G., and E. M. Rasmusson, 1985: The Southern Oscillation and El Niño. *Advances in Geophysics,* Vol. 28, Academic Press, 197–215.
Savage, M. L., C. R. Stearns, and G. A. Weidner, 1988: The Southern Oscillation signal in Antarctica. Preprints, *Second Conference on Polar Meteorology and Oceanography,* Madison, WI, Amer. Meteor. Soc., 141–144.
Shiotani, M., 1990: Low-frequency variations of the zonal mean state of the Southern Hemisphere troposphere. *J. Meteor. Soc. Japan,* **68,** 461–471.
Simmonds, I., and T. H. Jacka, 1995: Relationships between the interannual variability of Antarctic sea ice and the Southern Oscillation. *J. Climate,* **8,** 637–647.
Sinclair, M. R., 1994: An objective cyclone climatology for the Southern Hemisphere. *Mon. Wea. Rev.,* **122,** 2239–2256.
——, and X. Cong, 1992: Polar airstream cyclogenesis in the Australasian region: A composite study using ECMWF analyses. *Mon. Wea. Rev.,* **120,** 1950–1972.
Smith, S. R., and C. R. Stearns, 1993: Antarctic pressure and temperature anomalies surrounding the minimum in the Southern Oscillation index. *J. Geophys. Res.,* **98**(D7), 13 071–13 083.
Streten, N. A., and A. J. Troup, 1973: A synoptic climatology of satellite observed cloud vortices over the Southern Hemisphere. *Quart. J. Roy. Meteor. Soc.,* **99,** 56–72.
Taljaard, J. J., H. van Loon, H. L. Crutcher, and R. L. Jenne, 1969: Temperatures, dewpoints, and heights at selected pressure levels. Climate of the upper air: Southern Hemisphere. Rep. NAVAIR 50-IC-55, Chief of Naval Operations, Washington, DC, 135 pp.
Testa, J. W., G. Oehlert, D. G., Ainley, J. L. Bengtson, D. B. Siniff, R. M. Laws, and D. Rounsevell, 1991: Temporal variability in Antarctic marine ecosystems: Periodic fluctuations in the Phocid Seals. *Can. J. Fish. Aquat. Sci.,* **48,** 631–639.
Trenberth, K. E., 1976: Spatial and temporal variations of the Southern Oscillation. *Quart. J. Roy. Meteor. Soc.,* **102,** 639–653.
——, 1984: Interannual variability of the Southern Hemisphere circulation: Representativeness of the year of the Global Weather Experiment. *Mon. Wea. Rev.,* **112,** 108–123.
——, 1991: Storm tracks in the Southern Hemisphere. *J. Atmos. Sci.,* **48,** 2159–2178.
——, 1992: Global analyses from ECMWF and Atlas of 1000 to 10 mb circulation statistics. Tech. Note NCAR/TN-373 + STR, 191 pp.
Uccellini, L. W., 1990: Processes contributing to the rapid development of extratropical cyclones. *Extratropical Cyclones: The Erik Palmen Memorial Volume,* C. W. Newton and E. O. Holopainen, Eds., Amer. Meteor. Soc., 81–105.
van Loon, H., 1972: Wind in the Southern Hemisphere. *Meteor. Monogr.,* **13,** 87–100.
——, and R. A. Madden, 1981: The Southern Oscillation, Part I: Global associations with pressure and temperature in northern winter. *Mon. Wea. Rev.,* **109,** 1150–1162.
——, and D. J. Shea, 1985: The Southern Oscillation, Part IV: The precursors south of 15°S to the extremes of the oscillation. *Mon. Wea. Rev.,* **113,** 2063–2074.
——, and ——, 1987: The Southern Oscillation, Part VI: Anomalies of sea level pressure on the Southern Hemisphere and of Pacific sea surface temperature during the development of a warm event. *Mon. Wea. Rev.,* **115,** 370–379.
Vincent, D. G., 1985: Cyclone development in the South Pacific convergence zone during FGGE, 10–17 January 1979. *Quart. J. Roy. Meteor. Soc.,* **111,** 155–172.
——, 1994: The South Pacific convergence zone (SPCZ): A review. *Mon. Wea. Rev.,* **122,** 1949–1970.
——, and J. M. Schrage, 1994: Climatology of the TOGA-COARE and adjacent regions (1985–1990), Part 1: Kinematic variables. 104 pp. [Available from Dept. of Earth and Atmospheric Science, Purdue University, West Lafayette, IN 47907].
Walker, G. T., and E. W. Bliss, 1932: World weather V. *Mem. Roy. Meteor. Soc.,* **4,** 53–84.
Wang, B., 1992: The vertical structure and development of the ENSO anomaly mode during 1979–1989. *J. Atmos. Sci.,* **49,** 698–712.
——, 1995: Interdecadal changes in El Niño in the last four decades. *J. Climate,* **8,** 267–285.
Wu, G.-X., and B. Chen, 1990: Non-acceleration theorem in a primitive equation system. Part I. Acceleration of zonal mean flow. *Adv. Atmos. Sci.,* **15,** 1–21.